EUROPEAN ORGANIZATION FOR NUCLEAR RESEARCH

L3 Note 2760
July 4, 2002

Search for Single Top Production at LEP

The L3 Collaboration

Abstract

Single top production in e^+e^-annihilations is searched for in data collected by the L3 detector at centre-of-mass energies from 189 to 209 GeV, corresponding to a total integrated luminosity of 634 pb^{-1}. Investigating hadronic and semileptonic top decays, no evidence of single top production at LEP is obtained and upper limits on the single top cross section as a function of the centre-of-mass energy are found. Limits on possible anomalous couplings, as well as on the scale of contact interactions responsible for single top production are determined. These results are preliminary.

To be submitted to *Phys. Lett. B*

Introduction

One of the fundamental features of the Standard Model is that neutral currents are flavour diagonal, therefore any flavour changing neutral current (FCNC) process may occur only at second or higher orders through loops. The FCNC interactions of the top quark offer an ideal place to search for new physics and can be studied either in $\mathrm{t} \rightarrow \mathrm{qV}$ ($\mathrm{q} = \mathrm{u}, \mathrm{c}$; $\mathrm{V} = \gamma, \mathrm{Z}$) decays at the Tevatron or in single top production at LEP. In the Standard Model, the predicted rates of such processes are very small [1], but new physics beyond the Standard Model could lead to a significant increase. Enhancements of some orders of magnitude are predicted in two-Higgs-doublet models and supersymmetric models [2]. Flavour changing multiple-Higgs-doublet models bring further enhancements up to 10^{-5} [3], and models with FCNC coupled singlet quarks, compositeness or dynamical electroweak symmetry breaking [4] can yield a branching ratio of about 10^{-2}, in the reach of present colliders. The same considerations apply for the predicted single top production rates [5]. Experimental upper limits at the 95% confidence level on the FCNC branching fractions of the top quark were set by the CDF collaboration as $\mathrm{BR}(\mathrm{t} \rightarrow \mathrm{c(u)}\gamma) < 3.2\%$ and $\mathrm{BR}(\mathrm{t} \rightarrow \mathrm{c(u)Z}) < 33\%$ [6].

In this Letter, we consider two theoretical models for single top production $\mathrm{e^+e^-} \rightarrow \mathrm{t\bar{c}}$ + c.c: an approach which describes the process in terms of anomalous couplings, and an interpretation involving $[\mathrm{tce^+e^-}]$ contact interactions.

Single Top Production through Contact Interactions

An effective flavour changing vertex can be parameterized through $[\mathrm{tce^+e^-}]$ contact interactions [10]. The total unpolarised cross sections for $\mathrm{e^+e^-} \rightarrow \mathrm{t\bar{c}}$ + c.c. can be written as:

$$\sigma = \mathcal{C}\left[(3+\beta)(V_{LL}^2 + V_{RR}^2 + V_{RL}^2 + V_{LR}^2) + \frac{3}{2}(1+\beta)S_{RR}^2 + 8(3-\beta)T_{RR}^2\right] \tag{1}$$

where V_{ij}, S_{ij}, T_{ij} represent the coupling constants of vector, scalar and tensor fields, respectively (L and R stand for left-handed and right-handed fields), $\mathcal{C} = s/\Lambda^4 \times \beta^2/4\pi(1+\beta)^3$, $\beta = (s - m_\mathrm{t}^2)/(s + m_\mathrm{t}^2)$ and Λ is the energy scale parameter for the process. The predicted single top production cross sections are shown in Figure 1(b) for three different assumptions on the Lorentz structure of the $[\mathrm{tce^+e^-}]$ vertex. In this Letter, we give lower limits on the energy scale Λ. No directly comparable previous limits exist.

Anomalous Couplings

The Born-level cross section for the single top production process $\mathrm{e^+e^-} \rightarrow \mathrm{t\bar{c}}$ in the presence of anomalous couplings $\mathrm{tV\bar{c}}$, with $\mathrm{V} = \gamma, \mathrm{Z}$ [7], is give by:

$$\sigma = \frac{\pi\alpha^2}{s}\Big(1 - \mathcal{M}_\mathrm{t}\Big)^2\left[\frac{\kappa_\gamma^2 e_\mathrm{q}^2}{\mathcal{M}_\mathrm{t}}\Big(1 + 2\mathcal{M}_\mathrm{t}\Big) + \frac{\kappa_Z^2(1+a_\mathrm{W}^2)(2+\mathcal{M}_\mathrm{t})}{4\mathcal{S}_\mathrm{W}^2(1-\mathcal{M}_\mathrm{Z})^2} + \frac{3\kappa_Z\kappa_\gamma a_\mathrm{W} e_\mathrm{q}}{\mathcal{S}_\mathrm{W}(1-\mathcal{M}_\mathrm{Z})}\right] \tag{2}$$

in the limit of a massless c quark; κ_γ and κ_Z define the strength of the anomalous coupling for the current with a photon and a Z boson, respectively, s is the centre-of-mass energy squared, α is the fine structure constant, $e_\mathrm{q} = 2/3$ and m_t are the charge fraction and the mass of the top quark, $a_\mathrm{W} = 1 - 4\sin^2\theta_\mathrm{W}$, $\mathcal{S}_\mathrm{W} = \sin^2 2\theta_\mathrm{W}$, θ_W is the Weinberg angle, $\mathcal{M}_\mathrm{t} = m_\mathrm{t}^2/s$ and $\mathcal{M}_\mathrm{Z} = m_\mathrm{Z}^2/s$. QCD corrections can be taken into account following the prescriptions of Reference [8]. Moreover, the effect of initial state radiation (ISR) must be included. Born-level and QCD+ISR corrected predictions for the cross section are shown in Figure 1(a). The FCNC branching fraction limits set by CDF correspond to upper limits on the anomalous couplings of $\kappa_\gamma^2 < 0.176$ and $\kappa_Z^2 < 0.533$, at the 95% confidence level. Limits have been also set by searches at the LEP collider [9].

Data and Monte Carlo Samples

This study is based on 634 pb^{-1} of data collected by the L3 detector [11] at LEP at $\sqrt{s} = 189$ - 209 GeV. This integrated luminosity corresponds to the seven ranges of average centre-of-mass energies shown in Table 1.

$<\sqrt{s}>$ (GeV)	188.6	191.6	195.5	199.6	201.8	204.8	206.6
Luminosity (pb^{-1})	176.8	29.8	84.1	84.0	37.7	86.0	135.5
Error	0.4%	0.1%	0.1%	0.2%	0.1%	0.1%	0.1%

Table 1: Average centre-of-mass energies, their corresponding integrated luminosities and the relative error on the luminosity.

Crucial to this analysis is the prediction of Standard Model backgrounds, which rely on the following Monte Carlo (MC) programs: PYTHIA [12] and KK2f [13] for $\mathrm{q\bar{q}}$ final states, KORALW [14] for $\mathrm{W^+W^-}$ production, KORALZ [15] for $\tau^+\tau^-$ production, PHOJET [16] for two-photon interactions and EXCALIBUR [17] for other four-fermion final states. Single top production MC events have been generated with a modified version of PYTHIA [18]. QCD colour reconnection effects are taken into account in the framework of the Lund fragmentation model [19], forcing the top decay $\mathrm{t \rightarrow Wb}$ before the fragmentation takes place.

The response of the L3 detector is simulated using the GEANT [20] program, taking into account the effects of multiple scattering, energy loss and showering in the detector. Hadronic interactions in the detector are modeled using the GHEISHA [20] program. Time dependent detector inefficiencies, as monitored during the data taking period, are also simulated.

Analysis Procedures

In the reaction $\mathrm{e^+e^- \rightarrow t\bar{c}}$ at LEP centre-of-mass energies, the top quark is produced almost at rest and quickly decays via $\mathrm{t \rightarrow Wb}$ without forming top-flavoured hadrons. Depending on the subsequent decay of the W boson, the expected final state signatures are four jets ($\mathrm{t\bar{c} \rightarrow Wb\bar{c} \rightarrow qq'b\bar{c}}$) or two jets, one lepton and missing energy ($\mathrm{t\bar{c} \rightarrow Wb\bar{c} \rightarrow l\nu b\bar{c}}$), hereafter referred to as the hadronic and leptonic channels, respectively. In both channels, the c-quark energy E_c has a fixed value for a given $\sqrt{s}$:

$$E_\mathrm{c} \quad = \quad \frac{\sqrt{s}}{2}\left(1 - \frac{m_\mathrm{t}^2}{s}\right), \tag{3}$$

whereas the b-quark energy E_b has an almost fixed value which does not depend on $\sqrt{s}$, in the limit of a top quark at rest in the centre-of-mass frame:

$$E_\mathrm{b} \quad \simeq \quad \frac{m_\mathrm{t}}{2}\left(1 - \frac{m_\mathrm{W}^2}{m_\mathrm{t}^2}\right), \tag{4}$$

where m_{W} is the mass of the W boson. After hadronisation, the c and b quarks yield jets with almost fixed energies. Since both channels are characterised by the presence of a b quark, a clear signature exists and is exploited by using a b-jet tagging algorithm [21], which is mainly based on lifetime information.

Standard search procedures are applied to both the leptonic and hadronic channels. First, a pre-selection is applied which significantly reduces the background while keeping a high signal efficiency; this is especially effective against background from low multiplicity events and from two-photon interactions. Then, a further set of channel-specific selection criteria is chosen to increase the signal-to-background ratio. Finally, a discriminating variable is built using a neural-network technique.

Leptonic Channel

The signature for the leptonic channel is one energetic lepton, large missing momentum and two jets with a large difference in energy. The most energetic jet is assumed to be from the hadronisation of the b quark. The W-pair production $\mathrm{q\overline{q}}$ events and constitute the main background.

A pre-selection is applied requiring events to have at least 3 tracks, more than 15 calorimetric clusters and a visible energy of greater than $0.25 \times \sqrt{s}$, but less than $0.9 \times \sqrt{s}$. The presence of a well identified lepton is required; if there is more than one reconstructed lepton, the most energetic one is selected. An electron candidate is identified as a track with an associated cluster in the electromagnetic calorimeter; a muon candidate is reconstructed as a track in the central tracker matched to one in the muon spectrometer; a tau lepton is identified as a low-multiplicity jet. All clusters in the event, except the ones associated with the reconstructed lepton, are combined to form two hadronic jets using the DURHAM algorithm [22]. The jet axes and the missing momentum vector must be at least 15° and 26°, respectively, away from the beam axis.

To further reject background events, the energy of the lepton is required to be at least 10 GeV. The energy of the more energetic jet is required to exceed 60 GeV, whereas an upper bound is set on the lower energy jet, as detailed in Table 2. The width of the lower energy jet must be less than 0.4, the jet width being defined as the scalar sum of the transverse momenta of the jet clusters, normalised to the jet energy. The missing momentum is required to exceed 25 GeV, the lepton plus missing momentum invariant mass must be larger than 20 GeV and the two-jet invariant mass $M_{\mathrm{q\overline{q}}}$ has to lie outside a window around the W mass, as given in Table 2. The distributions of some relevant variables are shown in Figure 2. From the overall selection, 346 events are left in the data sample, with 357.0 expected from Standard Model backgrounds, while the signal efficiency is 10.6% (Table 3). In order to enhance the separation between signal

$\sqrt{s}$ (GeV)	189	192	196	200	202	205	207
Energy light jet (GeV) $\leq$	17.0	21.0	23.0	27.0	30.0	34.0	34.0
$\lvert M_{\mathrm{q\overline{q}}} - m_{\mathrm{W}} \rvert \geq$	14.0	11.0	8.5	6.0	6.0	3.0	3.0

Table 2: Centre-of-mass-energy-dependent cuts used for the leptonic channel, as described in the text

and background, a neural network technique [23] is then employed. The most important event variables are used as inputs to a neural network with 10 input nodes and two output nodes, $\mathcal{O}_{tc}$, $\mathcal{O}_{back}$, corresponding to the signal and the backgrounds, respectively. The input variables are related to the magnitude and direction of the missing momentum vector, the b-tag value, the two-jet and lepton-missing-momentum invariant masses. The final discriminating variable is then obtained as the product $\mathcal{O} = \mathcal{O}_{tc} \times (1 - \mathcal{O}_{back})$.

	Leptonic channel			Hadronic channel		
$\sqrt{s}$ (GeV)	Data	Back.	Sig. eff. (%)	Data	Back.	Sig. eff. (%)
189	10	13.6 ± 0.3	10.7 ± 0.2	95	76.6 ± 0.8	21.0 ± 0.4
192	3	4.6 ± 0.2	11.1 ± 0.3	14	14.3 ± 0.5	23.1 ± 0.6
196	23	21.1 ± 0.4	10.4 ± 0.3	43	38.7 ± 1.0	22.1 ± 0.6
200	35	40.5 ± 0.4	10.7 ± 0.3	37	38.1 ± 0.5	21.5 ± 0.6
202	22	23.7 ± 0.2	10.2 ± 0.3	19	19.4 ± 0.4	21.6 ± 0.6
204	104	99.1 ± 1.1	10.5 ± 0.3	50	41.1 ± 0.7	20.7 ± 0.6
207	149	154.4 ± 0.9	10.5 ± 0.3	63	59.7 ± 0.6	20.2 ± 0.5
All	346	357.0 ± 1.8	10.6 ± 0.1	321	287.9 ± 1.6	21.1 ± 0.2

Table 3: The number of data events for each centre-of-mass energy range, the expected number of background events and the Monte Carlo predicted signal efficiencies, for both the leptonic and hadronic channels. The errors are statistical only. The signal efficiency is for a top quark mass of 175 GeV. The corresponding W decay branching fraction is taken into account in the signal efficiency.

Hadronic Channel

The signature for the hadronic channel is four hadronic jets, two jets having an almost fixed energy and two being the decay products of a W. In addition, one jet must have a strong b-jet signature. The main backgrounds are W^+W^- production and QCD events.

A hadronic pre-selection, which requires a visible energy of at least $0.7 \times \sqrt{s}$ and an effective centre-of-mass energy larger than $0.85 \times \sqrt{s}$, is applied. The effective centre-of-mass is computed after having removed the photon radiation in the initial state. We also require more than 20 reconstructed tracks and more than two jets, built using the DURHAM algorithm with a resolution parameter $y_{cut} = 0.02$.

The events are forced into a four-jet topology by changing the value of y_{cut}. The c-jet candidate is defined as the jet whose energy is closest to the expected value (Equation (3)), assuming the expected top quark mass. Using the remaining three jets, the W boson is identified as the jet pair with invariant mass closest to the nominal W mass. The remaining jet is assumed to be the b jet.

By comparing the direction of the leading c quark in MC events with the c-jet defined as above, it is observed that the c selection purities are about 49%, 53% and 60% for $\sqrt{s} = 189$, 192 and 196 GeV, respectively, and approach the limit of 62% for $\sqrt{s} \geq 200$ GeV.

A neural network with 24 input nodes and 3 output nodes is then used. The neural network inputs variables are related to such jet characteristics as their energies and masses, the b-tag discriminant of the b jet candidate and various event shapes variables. Some of these distributions are shown in Figures 3(a) and (b). One network output selects the signal and is used as the final discriminating variable. The other two outputs, which tag $q\bar{q}$ and W^+W^- events, are used to further reject the background by applying a cut of 0.1 and 0.3, respectively. Their distributions are shown in Figure 3(c) and (d). After all cuts, the final sample consists of 321 data events, to be compared with 287.9 expected background events, and a 21.1% signal efficiency, as detailed in Table 3.

Study of Systematic Uncertainties

The single top search described in this Letter relies on the comparison between data and Monte Carlo simulations. The main systematic uncertainties on the cross section upper limit, related to background, signal and detector simulations, are given in Table 4. No systematic uncertainty is assigned to the top quark mass variation, as all the results are parameterised in terms of this quantity.

Effect j	$< \Delta\sigma_j >$	Effect j	$< \Delta\sigma_j >$
Stat. MC back.	0.4	Luminosity	$<$ 0.1
Stat. MC sig.	1.7	Lepton Id	0.1
$q\bar{q}$ back. modelling	0.2	Event shape	0.9
W^+W^- back. modelling	$<$ 0.1	Energy res.	1.6
ZZ back. modelling	0.4	b-tagging	1.4
Signal angular distr.	2.0	Other back. modelling	0.5

Table 4: Systematic errors on the single top cross section in percent.

For each effect j, $< \Delta\sigma_j >$ is the mean on $\sqrt{s}$ of $(|\sigma_0 - \sigma_j|)/\sigma_0$, where σ_0 is the reference limit on the single top cross section and σ_j is the limit found after having applied a systematic correction to the background or to the signal. For the MC statistical effects, the selection efficiency was corrected by a factor $1/\sqrt{N}$, N being the number of MC events after the selection. For the $q\bar{q}$, W^+W^- and ZZ background modelling, the corresponding cross section was corrected by 2%, 0.5% and 10%, respectively. To study the systematic effect arising from variations of the signal final state angular distributions,various samples were simulated, inside the limits allowed in the anomalous coupling scenario. The variation into the selection efficiency was found to be no more than 0.6%. The error on the L3 measurement of the luminosity was used (Table 1). For the remaining effects - lepton identification, event shape, energy resolution, b-tagging and other background modelling - we applied a correction method which consists, in performing a correction for each associated group of input variables in order to match the background to the data distributions.

Results

The distributions of the leptonic and hadronic discriminating final variables are shown in Figure 4. A very good discrimination between signal and background is achieved. No significant deviation from the Standard Model background expectation is observed. The combined 95% confidence level upper limits on the single top total cross section are found [24] and listed in Table 5. For these limits, the branching ratio for the top decay is assumed to be saturated by $t \rightarrow Wb$. The limits are obtained for the signal process $e^+e^- \rightarrow t\bar{c}$, a deterioration of the limits of about 10% is found for the corresponding process $e^+e^- \to t\bar{u}$. Table 6 lists the 95% confidence level lower limit on the energy scale parameter Λ of a possible $[tce^+e^-]$ contact interaction, described in Equation (1). Referring to the anomalous-coupling formalism described in Reference [7], and using the cross section expression of Equation (2) with QCD and ISR corrections, an exclusion region in the κ_γ vs. κ_Z plane is obtained, as displayed in Figure 5(a). Flavour changing decays of the top quark through anomalous vertices are taking into account in the iterative limit computation. Using the Born-level cross section of Equation (2), a corresponding exclusion region in the BR($t \to Zq$) vs. BR($t \to \gamma q$) plane is found, as shown in Figure 5(b). The anomalous-coupling formalism upper limits are summarised in Table 7.

$<\sqrt{s}>$	(GeV)	189	192	196	200	202	205	207
$\sigma_{95}(m_t = 170$ GeV$)$	(pb)	0.36	0.87	0.77	0.54	0.62	0.63	0.51
$\sigma_{95}(m_t = 175$ GeV$)$	(pb)	0.22	0.73	0.67	0.45	0.56	0.51	0.39
$\sigma_{95}(m_t = 180$ GeV$)$	(pb)	0.21	0.75	0.64	0.42	0.52	0.48	0.37

Table 5: Measured 95% confidence level upper limits on the total cross section for single top production as a function of the centre-of-mass energy. The limits are given for three assumptions on the top quark mass.

	$V_{ij} = 1$	$S_{RR} = 1$	$T_{RR} = 1$
Λ (TeV)	0.76 / 0.75 / 0.70	0.65 / 0.65 / 0.60	1.24 / 1.24 / 1.16

Table 6: Measured 95% confidence level lower limits on the energy scale parameter Λ in TeV. Three different scenarios for the coupling constants are considered: ($V_{ij} = 1$, $S_{RR} = 0$, $T_{RR} = 0$); ($V_{ij} = 0$, $S_{RR} = 1$, $T_{RR} = 0$); ($V_{ij} = 0$, $S_{RR} = 0$, $T_{RR} = 1$). The limits are given for three values of the top quark mass : 170/175/180 GeV.

κ_Z	=	0.31 / 0.34 / 0.40	BR($t \to Zq$)	=	12.4% / 12.2% / 15.7%
κ_γ	=	0.36 / 0.40 / 0.47	BR($t \to \gamma q$)	=	4.0% / 3.7% / 4.5%

Table 7: Measured 95% confidence level upper limits on the anomalous-coupling parameters κ_γ and κ_Z and on the FCNC top decay branching fractions. The limits are given for three values of the top quark mass : 170/175/180 GeV. In each case, for the limit on κ_γ or κ_Z, the other parameter is assumed to be 0.

References

[1] G. Eilam, J.L. Hewett and A. Soni, Phys. Rev. **D44** (1991) 1473; C.S. Huang, X.H. Wu and S.H. Zhu, Phys. Lett. **B452** (1999) 143.

[2] C.S. Li, R.J. Oakes and J.M. Yang, Phys. Rev. **D49** (1994) 293; R.S. Chivukula, E.H. Simmons and J. Terning, Phys. Lett. **B 331** (1994) 383; J.L. Lopez, D.V. Nanopoulos and R. Rangarajan, Phys. Rev. **D56** (1997) 3100.

[3] T.P. Cheng and M. Sher, Phys. Rev. **D35** (1987) 3484; B. Mukhopadhyaya and S. Nandi, Phys. Rev. Lett. **66** (1991) 285; W.S. Hou, Phys. Lett. **B 296** (1992) 179; L. Hall and S. Weinberg, Phys. Rev. Rapid Comm. **D48** (1993) R979; M. Luke and M.J. Savage, Phys. Lett. **B 307** (1993) 387; D. Atwood, L. Reina and A. Soni, Phys. Rev. **D55** (1997) 3156.

[4] V. Barger, M.S. Berger and R.J.N. Phillips, Phys. Rev. **D52** (1995) 1663; H. Georgi *et al.*, Phys. Rev. **D51** (1995) 3888; C.T. Hill, Phys. Lett. **B 345** (1995) 483; B. Holdom, Phys. Lett. **B 351** (1995) 279; J. Berger *et al.*, Phys. Rev. **D54** (1996) 3598; B.A. Arbuzov and M.Y. Osipov, Phys. Atom. Nucl. **62** (1999) 485.

[5] E. Boos, M. Dubinin, A. Pukhov, M. Sachwitz and H.J. Schreiber, Eur. Phys. J. **C21** (2001) 81; S. Bar-Shalom *et al.*, Phys. Rev. **D57** (1998) 2957; D. Atwood, L. Reina and A. Soni, Phys. Rev. **D53** (1996) 1199; M. Chemtob and G. Moreau, Phys. Rev. **D59** (1999) 116012; U. Mahanta and A. Ghosal, Phys. Rev. **D57** (1998) 1735.

[6] The CDF collaboration, F. Abe *et al.*, Phys. Rev. Lett. **80** (1998) 2525.

[7] V.F. Obraztsov, S.R. Slabospitsky and O.P. Yushchenko, Phys. Lett. **B 426** (1998) 393; T. Han and J.L. Hewett, Phys. Rev. **D60** (1999) 074015.

[8] L.J. Reinders, H. Rubinstein and S. Yazaki, Phys. Rep. **127** (1985) 1.

[9] The ALEPH Collaboration, Preprint CERN-EP/2002-042 (2002); The OPAL Collaboration, Phys. Lett. **B 521** (2001) 181.

[10] S. Bar-Shalom and J. Wudka, Phys. Rev. **D60** (1999) 094016.

[11] L3 Collaboration, B. Adeva *et al.*, Nucl. Inst. Meth. **A 289** (1990) 35.

[12] T. Sjöstrand, Preprint CERN-TH/7112/93 (1993).

[13] S. Jadach, B.F.L. Ward and Z. Wąs, Comp. Phys. Comm. **130** (2000) 260.

[14] M. Skrzypek *et al.*, Comp. Phys. Comm. **94** (1996) 216.

[15] S. Jadach, B.F.L. Ward and Z. Wąs, Comp. Phys. Comm. **79** (1994) 503.

[16] R. Engel and J. Ranft, Phys. Rev. **D54** (1996) 4244.

[17] F.A. Berends, R. Pittau and R. Kleiss, Comp. Phys. Comm. **85** (1995) 437.

[18] L. Cuénoud, Générateurs de Flavour Changing Neutral Currents, Travail de diplôme, Université de Lausanne, 1996.

[19] B. Andersson *et al.*, Phys. Rep. **97** (1983) 31.

[20] R. Brun *et al.*, Preprint CERN-DD/EE/84-1 (1994); H. Fesefeldt, Preprint RWTH Aachen PITHA 85/02 (1985).

[21] L3 Collaboration, M. Acciarri *et al.*, Phys. Lett. **B 411** (1997) 373.

[22] S. Catani *et al.*, Phys. Lett. **B 269** (1991) 432; S. Bethke *et al.*, Nucl. Phys. **B 370** (1992) 310.

[23] L. Lönnblad, C. Peterson and T. Rögnvaldsson, Nucl. Phys. **B 349** (1991) 675; C. Peterson *et al.*, Comp. Phys. Comm. **81** (1994) 185.

[24] V. F. Obraztsov, Nucl. Inst. Meth. **A 316** (1992) 388.

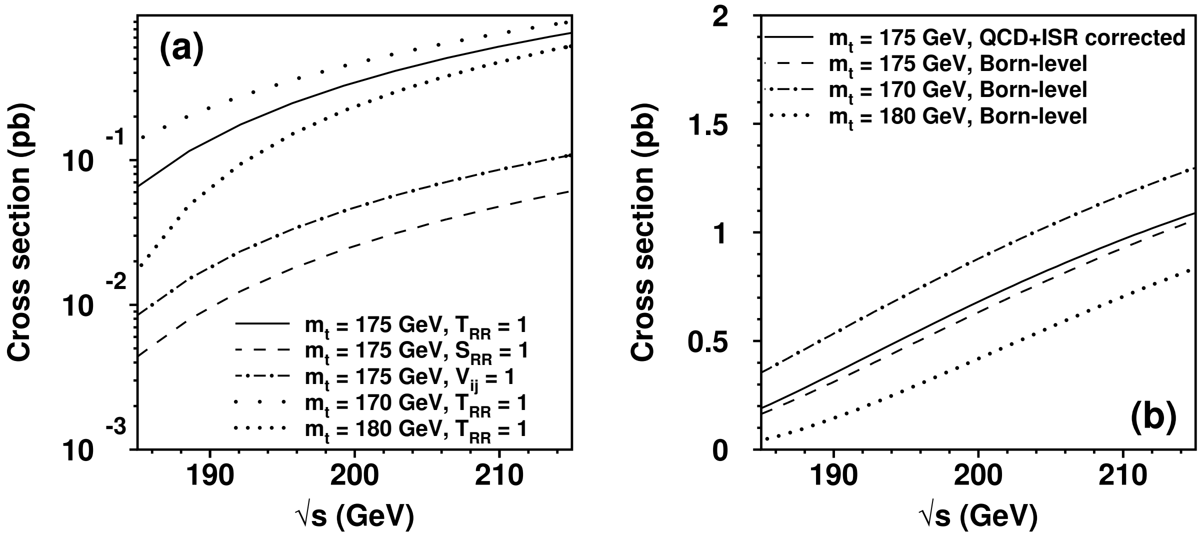

Figure 1: Theoretical total cross section for single top production versus centre-of-mass energy for three different top quark mass values. (a) For $[tce^+e^-]$ contact interactions with several different assumptions on the Lorentz structure and an energy scale parameter $\Lambda = 1$ TeV. (b) From the model described in Equation (2). CDF limits on the values for the anomalous constants are assumed.

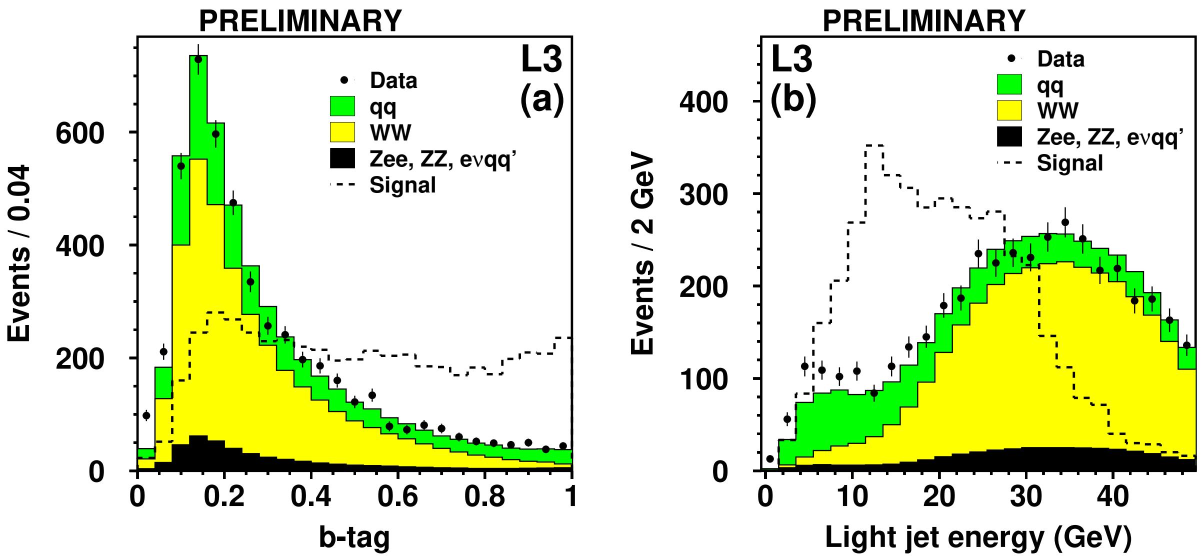

Figure 2: Distributions for the leptonic channel of (a) the b-tag discriminant variable for the more energetic jet, and (b) the energy of the lower-energy jet. Data from all centre-of-mass energies are included. The signal histogram is for a top quark mass of 175 GeV and is normalised to the number of data events. The background from $q\bar{q}$, W^+W^- and 4-fermion processes are shown separately.

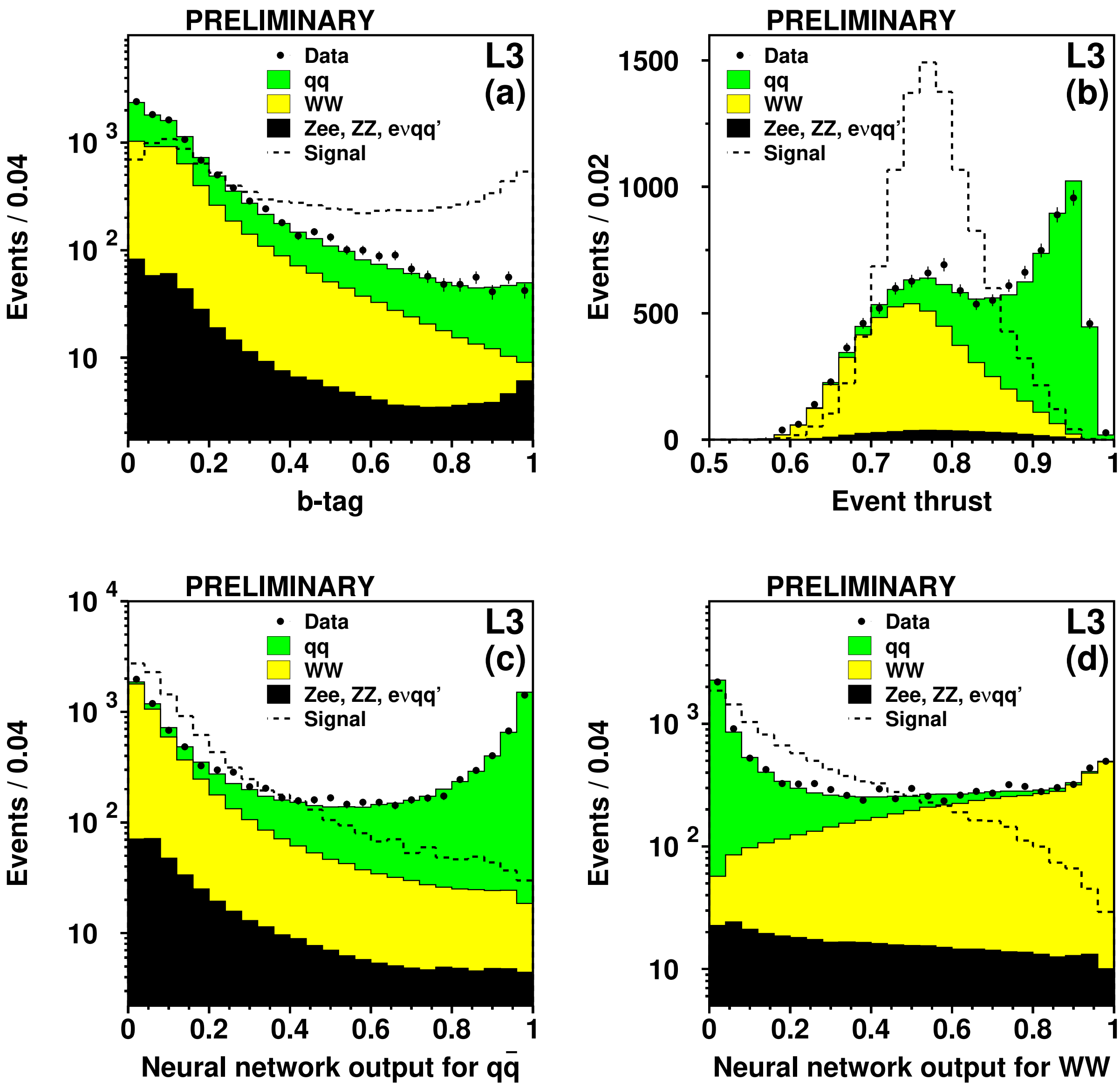

Figure 3: Distributions for the hadronic channel after pre-selection of (a) the b-tag variable of the b jet, (b) the event thrust and (c), (d) the neural network outputs related to q$\overline{\text{q}}$ and WW backgrounds. Data from all centre-of-mass energies are included. The signal histogram is for a top quark mass of 175 GeV and is normalised to the number of data events. The background from q$\overline{\text{q}}$, W^+W^- and 4-fermion processes are shown separately.

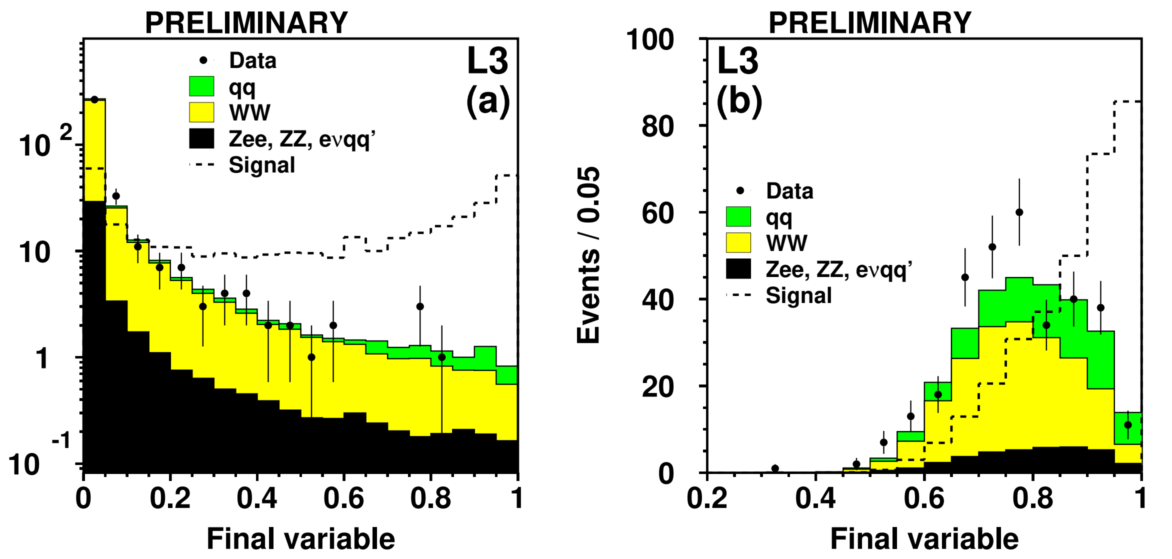

Figure 4: Distribution of the final discriminating variable for (a) the leptonic channel and (b) the hadronic channel. Data from all centre-of-mass energies are included. The signal histogram is for a top quark mass of 175 GeV and is normalised to the number of data events. The background from $q\bar{q}$, W^+W^- and 4-fermion processes are shown separately.

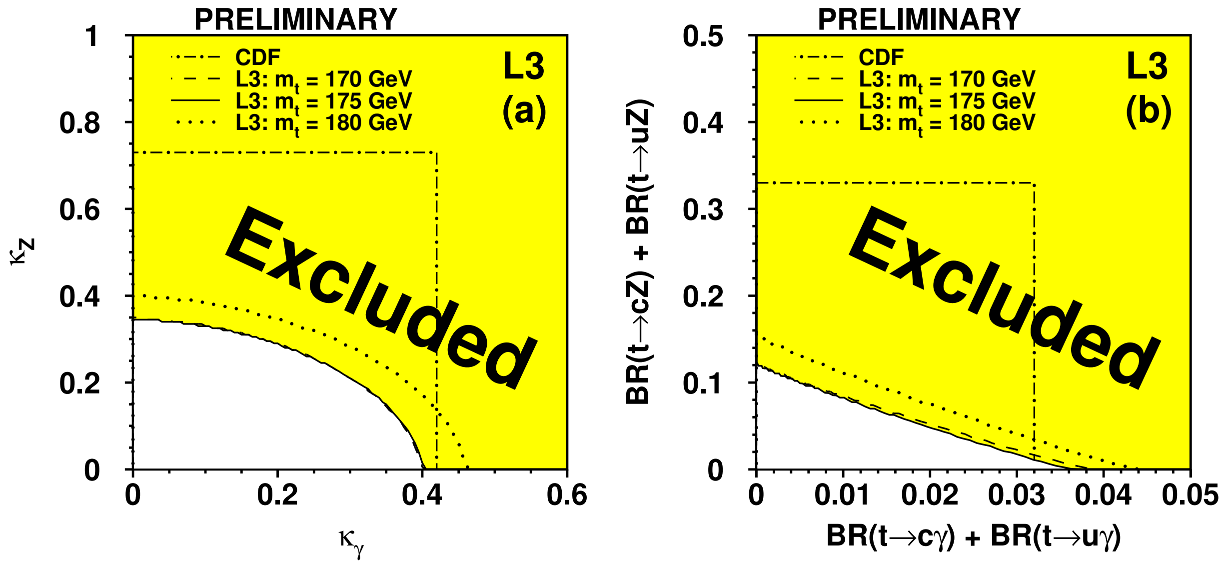

Figure 5: Exclusion regions at the 95% confidence level in (a) the k_γ vs. k_Z plane and (b) the BR($t \rightarrow \gamma q$) vs. BR($t \rightarrow Zq$) plane for three different values of the top quark mass. The CDF exclusion domain is also shown. Equation (2) has been used, neglecting the interference term.